International Journal of Mining Science and Technology 29 (2019) 513–519

Contents lists available at ScienceDirect

International Journal of Mining Science and Technology

journal homepage: www.elsevier.com/locate/ijmst

Preparation of magnetically separable mesoporous activated carbons from brown coal with Fe_3O_4

Yong Jiang [a,*], Qiang Xie [b], Yanhai Zhang [a], Cuiyu Geng [a], Bin Yu [a], Juan Chi [a]

[a] Poten Environmental Group Co. Ltd., Beijing 100083, China
[b] School of Chemistry and Environmental Engineering, China University of Mining and Technology (Bejing), Bejing 100083, China

ARTICLE INFO

Article history:
Received 11 January 2018
Received in revised form 26 March 2018
Accepted 9 January 2019
Available online 14 January 2019

Keywords:
Magnetic activated carbon
Preparation
Brown coal
Ferroferric oxide
Magnetic separation

ABSTRACT

Magnetically separable mesoporous activated carbon was prepared from brown coal in the presence of Fe_3O_4 as a bi-functional additive. Magnetic activated carbon (MAC) was characterized by low-temperature nitrogen adsorption, scanning electron microscopy (SEM), transmission electron microscopy (TEM), X-ray diffraction (XRD), X-ray photoelectron spectroscopy (XPS) and vibrating sample magnetometry (VSM). The evolution behaviors and transition mechanism of Fe_3O_4 during the preparation of MAC were investigated. The results show that prepared MAC with 6 wt% Fe_3O_4 addition having a specific surface area and mesopore ratio of 370 $m^2 \cdot g^{-1}$ and 55.7%, which meet the requirements of adsorption application and magnetic recovery. Highly dispersed iron-containing aggregates with the size of 0.1 μm in the MAC were observed. During the preparation of MAC, Fe_3O_4 could enhance the escape of volatiles during the carbonization. Fe_3O_4 could also accelerate burning off the carbon wall during activation, which leads to enlarging micropore size, then resulting in the generation of mesopore and macropore. As a result, a part of Fe_3O_4 converted into FeO, FeOOH, α-Fe, γ-Fe, Fe_2SiO_4 and compound of Aluminum-iron-silicon. The prepared activated carbon, which was magnetized by both of residual Fe_3O_4, reduced α-Fe and γ-Fe, can be easily separated from the original solution by external magnetic field.

1. Introduction

Mesoporous activated carbon which has been widely used in the applications of catalyst supports, capacitors and biomedical engineering often involves large molecules or macromolecules as adsorbates [1–6]. During the adsorption process, large size particle of activated carbon changed into fine particles resulting from interactive collision or attrition. However, it is difficult to effectively separate these fine particles by traditional recovery methods such as gravitational sedimentation, centrifugation, filtration, and flotation. This is because these processes are inefficient and time-consuming. It is significantly important to effectively separate and recover these fine activated carbon particles in the expensive metal (such as gold) extraction processes as well as activated carbon industry [7]. The separation of fine activated carbon particles from aqueous solutions by magnetic separation technique to be a viable process is a relatively cheap, effective and fast removal method [8]. Therefore, the magnetization of activated carbon is the vital step for the magnetic recovery process.

Preparation of MAC has recently became a hot topic in the activated carbon industry, metallurgy, and environmental, chemical and pharmaceutical areas [9–11]. Traditionally, using commercial microporous activated carbon as precursor, MAC was prepared in the presence of $FeCl_3$ [12], $Fe(NO_3)_3$ [13], $Ni(NO_3)_2$ [14], Fe_3O_4 or γ-Fe_2O_3 [15,16], and Fe with Co and Ni alloy [17] etc. as a magnetization reagent by adsorption, bonding, mixing and grinding processes [11,15]. Ao et al. [18] prepared a MAC by co-precipitation of $FeSO_4$ and $FeCl_3$ solution with NH_4OH using a developed microporous activated carbon as a precursor. The surface area of MAC was 870 m^2/g, which was lower than the original activated carbon with a surface area of 1093 m^2/g. Wang et al. [19] reported a MAC using Mn-Zn ferrite as magnetization reagent. When compared to original activated carbon, the surface area and pore volume of MAC reduced 55% and 19%, respectively. This kind of MAC has a feature of small surface area and very poor porosity compared to common activated carbon. This is because partial pores were blocked by the magnetic particles. Meanwhile, the magnetic stability was poor due to the weak physical interaction between magnetic particles and activated carbon matrix. Therefore, immobilization of magnetic particles in the activated carbon, while at the same time keeping a high surface area and developed pore structure, is the key point for the preparation of MAC.

* Corresponding author.
E-mail address: Yong.jiang@poten.cn (Y. Jiang).

https://doi.org/10.1016/j.ijmst.2019.01.002
2095-2686/

A simple one-step method for the preparation of MACs with different surface area and porosity with the presence of Fe, Ni, and Mn compounds such as iron oxide, $Ni(NO_3)_2$ has recently been published by our team [14,16]. However, the evolution behaviors and transition mechanism of Fe_3O_4 during the preparation of mesoporous MAC were not investigated in depth. In this work, the preparation of MAC with developed mesoporous structure and relative magnetic ability was described. The brown coal was used as carbonaceous raw material and Fe_3O_4 was applied as a bi-functional additive. Meanwhile, the mechanism of transition of Fe_3O_4 and magnetization of MAC were analyzed in detail.

2. Experimental

2.1. Materials

The deliming brown coal sample was obtained from Baorixile Coal Co., Ltd in the Inner-Mongolia of China. Results of proximate and ultimate analyses of brown coal sample were shown in Table 1. And chemical analysis result of ash in the brown coal was shown in Table 2. High-temperature coal tar as binder and Fe_3O_4 (less 46 μm) as a bi-functional additive were selected for the preparation of MACs.

2.2. Sample preparation

Powdered brown coal (particle diameter less 75 μm) was mixed well with a weighed portion of Fe_3O_4 from 0% to 8% in 2% increments, denoted as 0%, 2%, 4%, 6% and 8%. 40 wt% high temperature coal tar, 10 wt% distilled water was added to the former mixture and then stirred vigorously. The thoroughly mixed feedstock was extruded in the form of 1 cm cylinder.

These cylinders were air dried and then carbonized in a horizontal furnace at a heating rate of 5 °C/min from room temperature to 650 °C and then maintained for 45 min. Then 60 g char sample was continuously heated to 850 °C with a heating rate of 10 °C/min and a steam activation with a vapor flow of 0.77 mL $H_2O{\cdot}(g{\cdot}h)^{-1}$ based on the char was carried out at 850 °C for 120 min. Resultant MAC samples were named as MAC-0, MAC-2, MAC-4, MAC-6 and MAC-8 according to the adding amount of Fe_3O_4. MC-0 represents a char sample corresponding to MAC-0.

2.3. Characterization

The proximate and ultimate analyses of brown coal were carried out according to Chinese Standards of GB/T 212-2008 and GB/T 476-2001 by an automatic coal proximate analyzer (TGA701) and an element analyzer (Vario MACROCHNS). The specific surface area of MACs was obtained by low temperature nitrogen adsorption (at 77 K), using a micromeritics (ASAP 2010 M). The *t*-plot method was applied to calculate the micropore volume (V_{micro}). Micropore and Mesopore distribution were determined by HK method and the Barrett, Joyner and Halenda (BJH) theory. The mesopore volume (V_{meso}) was calculated by subtracting V_{micro} from total volume (V_{total}). The mesopore ratio was defined as $V_{meso}/V_{total} \times 100\%$. The morphology of samples was characterized with a scanning electron microscope (S-360) and a transfer electron microscope (H-7500). The structural properties were determined by X-ray diffractometer (XRD) using Cu Kα radiation (D/MAX-RB). X-ray photoelectron spectroscopy (XPS) measurements were carried out on a JPS-9000MC (JEOL) with monochromatic Mg Kα radiation (1253 eV) under 7×10^{-7} Pa. The indium paper was as a foil to avoid the influence of iron substrate support and the samples were pressed on the surface of indium paper. The argon-ion sputtering could not be employed because partial Fe^{3+} can be reduced to Fe^{2+} [20]. The conditions used for the high-resolution spectra were as follows: pass energy 10 eV, step size 0.025 eV and 400 scan times. The magnetic measurements were carried out with a vibrating sample magnetometer (VSM-7307).

3. Results and discussion

3.1. Morphologies of MACs

The SEM photographs of CM-0 and MACs were shown in Fig. 1. MACs had a surface morphology of sheet-like graphite packing structure that shows which make a large number of micropores. For all MACs, small aggregates were observed, which appear brighter and supported on the darker surface of the activated carbon. The fine iron oxide particles tend to cover the surface of activated carbon instead of being dispersed uniformly over the entire surface. As addition amount of Fe_3O_4 increase, the aggregates on the surface of MACs increase. By Energy-dispersive X-Ray (EDX) analysis (not shown), it confirmed that the aggregates was an iron-containing compound. The iron content of the samples was shown in the upper right corner of each picture in Fig. 1.

Fig. 2 shows the TEM images of MAC-0 and MAC-6. It can be seen that the color of MAC-0 was uniform. Compared with MAC-0, a lot of black spots fixed on the MAC-6 were found after 6 wt% Fe_3O_4 was added. These black spots were iron-containing compounds whose size was about 0.1 μm (see Fig. 2b).

3.2. Surface area and pore volume of MACs

3.2.1. Nitrogen isotherm

Fig. 3 shows the nitrogen adsorption-desorption isotherms of MACs. It can be seen that the isotherms of all MACs were belonged to type Ⅳ isotherms with hysteresis loop according to the IUPAC classification, suggesting that the MACs have mesopores [21]. As

Table 1
Characterization of brown coal.

Proximate analysis (wt%)				Ultimate analysis (wt%)				
M_{ad}	A_d	V_{daf}	FC_{daf}	C_d	H_d	N_d	O_d^*	S_{td}
27.26	7.82	48.78	51.22	73.91	3.98	0.88	20.75	0.49

Note: *By difference; M_{ad} means moisture content as received basis; A_d means ash content as dry basis; V_{daf} means volatile content as dry ash free basis; FC_{daf} means fixed carbon content as dry ash free basis.

Table 2
Chemical analysis of ash of brown coal.

Composition	SiO_2	Al_2O_3	Fe_2O_3	TiO_2	CaO	MgO	K_2O	Na_2O	P_2O_5	MnO_2	SO_3
Value (wt%)	42.80	12.78	15.42	0.61	15.64	2.84	0.33	0.76	0.08	0.98	1.15

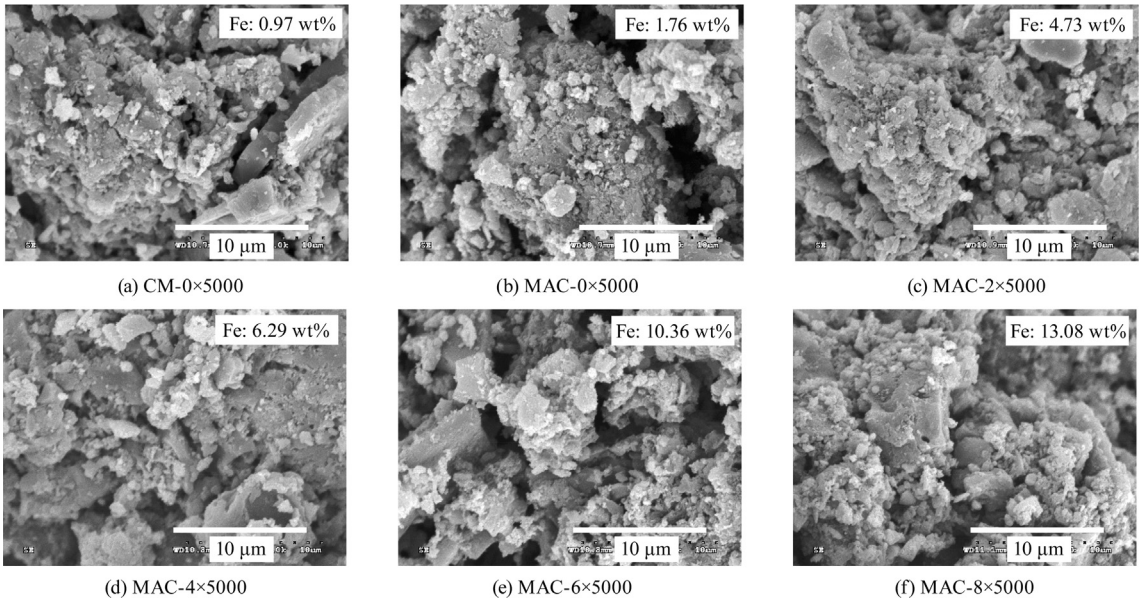

Fig. 1. SEM photographs of CM-0 and MACs.

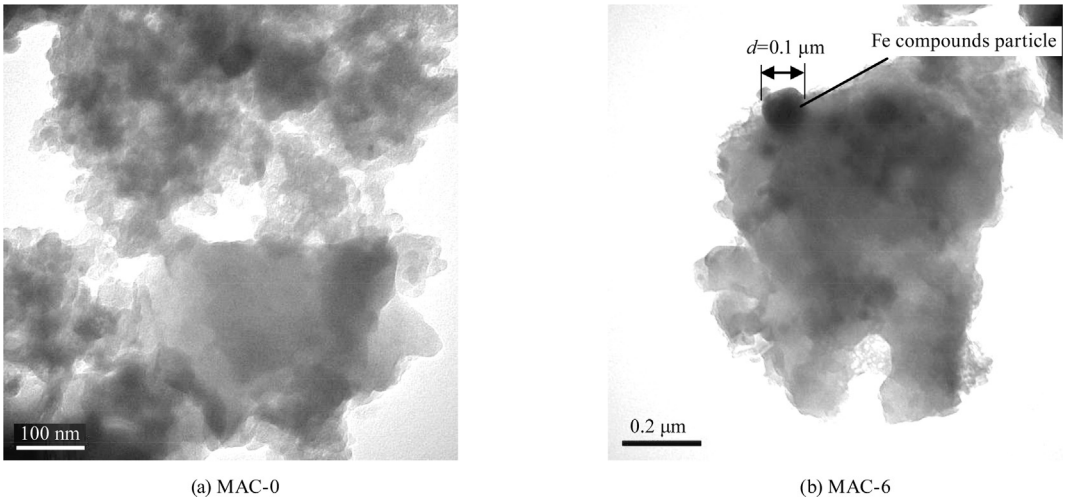

Fig. 2. TEM images of MAC-0 and MAC-6.

increasing additive amount of Fe_3O_4, the isotherms of MACs were lower than that of MAC-0, indicating that the specific surface area decreased and pores were enlarged.

3.2.2. Specific surface area and pore volume

The pores of a porous material are classified into three groups: micropores (d < 2 nm), mesopores (2 nm < d < 50 nm) and macropores (d > 50 nm) according to the International Union of Pure and Applied Chemistry (IUPAC) [21]. The specific surface area and pore volume of MACs with different amount of Fe_3O_4 were shown in Table 3. It was found that the specific surface area and total pore volume of MACs decreased after adding Fe_3O_4. When addition amount of Fe_3O_4 was 6%, the specific surface area, average pore diameter and total pore volume of MAC have a minimum of 370 $m^2 \cdot g^{-1}$, 2.83 nm and 0.262 $cm^3 \cdot g^{-1}$, respectively. It is noteworthy that the mesopore ratio of MAC-6 reached the maximum of 55.7%.

The pore size distribution of MACs was shown in Fig. 4. The MACs have a narrow pore size distribution that the pore diameter of micropore centered at ca. 1.4–1.6 nm and pore diameter of mesopore centered at ca. 3.0–4.5 nm. The micropore diameter of MACs was slightly increased after addition of Fe_3O_4 due to Fe_3O_4 could accelerate the burn off of carbon wall resulting in partial micropore was enlarged into mesopore and macropore. As the consequence, the specific surface area and the total volume of MACs reduced in comparison with MAC-0.

3.3. Structural analyses of MACs

3.3.1. XRD analysis of MACs

XRD patterns of MACs were shown in Fig. 5. Two broad diffraction peaks in the range of 10°–30° and 40°–50° were appeared corresponding to the (0 0 2) and (1 0 0) of crystal graphite [22]. The peaks of Fe_3O_4, FeO and Fe_2SiO_4 were obviously distinguished and shown in Fig. 5. The peaks at 44.7°, 65.0° and 82.3° were assigned to α-Fe, and the peaks at 43°, 49°, 65° and 77° were assigned to γ-Fe [23], but their intensities were very low. The

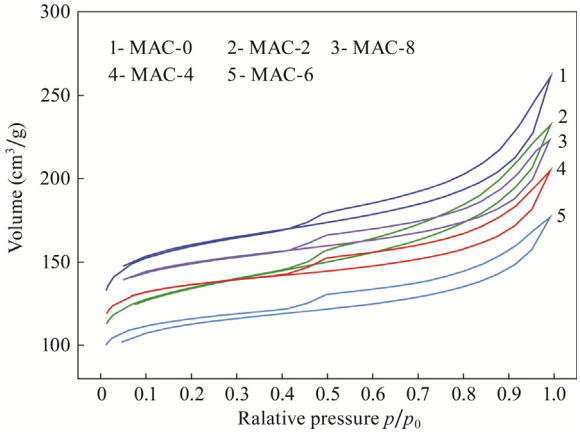

Fig. 3. The adsorption and desorption of isotherms of MACs.

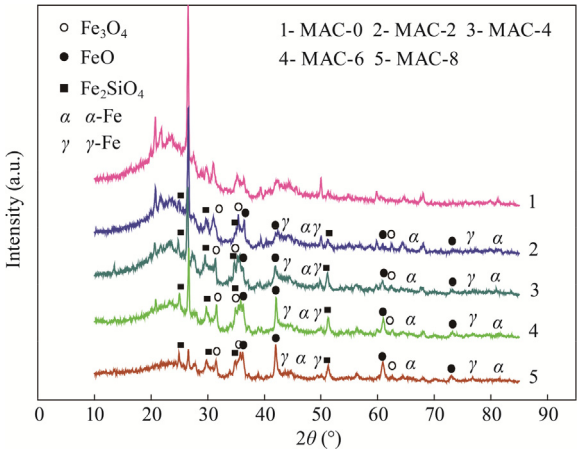

Fig. 5. XRD patterns of MACs.

species of iron-containing compound were demonstrated by XPS analysis in the next section.

The peaks (0 0 2) of crystal graphite became more flat as increasing addition amount of Fe_3O_4 in MACs, suggesting the increase of anisotropic constituents in chars. The parameters of graphitic crystallites [24] of MACs were illustrated in Table 4. The average diameter of crystallite *La* increased and height of crystallite *Lc* decreased with the increase of the amount of Fe_3O_4, this means that Fe_3O_4 could accelerate burn off of carbon wall and enhance the condensation reaction between carbon and carbon [25]. It is important to note that the interlayer spacing $d_{(0\,0\,2)}$ of MACs changed so slightly. Since the particle size of Fe_3O_4 was about 46 μm and it could not be able to penetrate into the carbon interlayers, then the effect of Fe_3O_4 on the interlayer can be ignored.

3.3.2. XPS analysis of MACs

X-ray photoelectron spectroscopy (XPS) is a versatile surface analysis technique that can be utilized to analyze the states of iron oxide. Fig. 6 shows the survey scans and high-resolution XPS spectra of the Fe2P region of MACs. The survey scans spectra shows that $Fe2P_{1/2}$ and $Fe2P_{3/2}$ which demonstrated that Fe was fixed on the surface of MACs. This result was in agreement with XRD and TEM analysis. Meanwhile, it can be found that the peaks of $Fe2P_{3/2}$ can be decomposed into three contributions corresponding to the different oxidation of iron. The main contribution is attributed to FeOOH (binding energy at 711.5 eV), and other contributions were assigned to α-Fe_2O_3 (binding energy at 710.8 eV), Fe_3O_4 (binding energy at 710.5 eV) and metal Fe (binding energy at 706.7 eV) [26].

3.4. Magnetic properties of MACs

The hysteresis loop of MACs was shown in Fig. 7. The magnetic parameters such as saturation magnetization M_S, coercivity H_C, and remanence M_r were listed in Table 5. The saturation magnetization *Ms* of MACs reduces firstly and increases afterward as the amount

Table 3
Parameters of the specific surface area and pore volume of MACs.

Sample	Specific surface area ($m^2 \cdot g^{-1}$)	Average pore diameter (nm)	Total pore volume ($cm^3 \cdot g^{-1}$)	Micropore volume ($cm^3 \cdot g^{-1}$)	Mesopore volume (V_{total}–V_{micro}, $cm^3 \cdot g^{-1}$)	Mesopore ratio (V_{meso}/V_{total}, %)
MAC-0	525	2.91	0.383	0.206	0.177	46.2
MAC-2	434	3.17	0.344	0.157	0.187	54.4
MAC-4	436	2.77	0.302	0.186	0.116	38.4
MAC-6	370	2.83	0.262	0.146	0.116	55.7
MAC-8	488	2.75	0.335	0.200	0.135	40.3

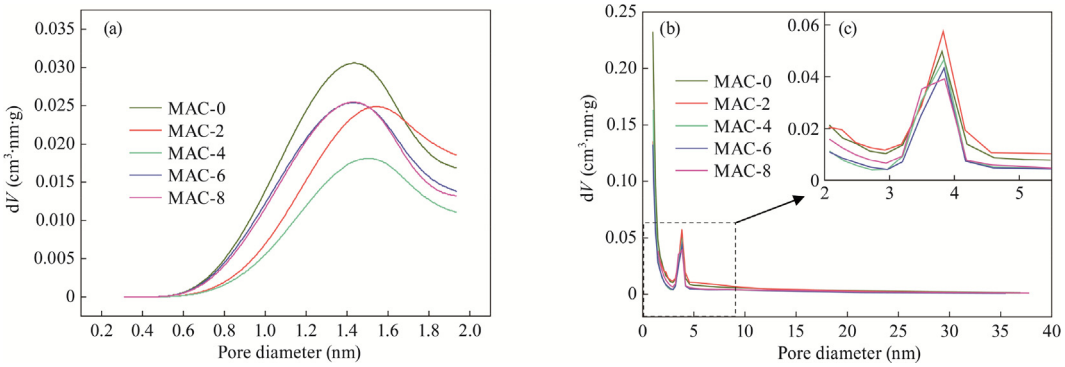

Fig. 4. Pore size distributions of MACs: (a) micropore, (b) mesopore and (c) drawing of partial enlargement.

Table 4
Parameters of graphitic crystallites of MACs.

Sample	2θ (°)		Full width at half maximum (FWHM) (°)		Parameters of graphitic crystallites (nm)		
	(0 0 2)	(1 0 0)	(0 0 2)	(1 0 0)	Interlayer spacing $d_{(0\,0\,2)}$	Diameter of crystallite *La*	Height of crystallite *Lc*
MAC-0	23.09	43.20	7.25	3.50	0.3849	4.9910	1.1184
MAC-2	23.12	43.02	7.50	2.42	0.3844	7.2138	1.0812
MAC-4	22.98	43.18	6.95	3.28	0.3867	5.3253	1.1664
MAC-6	22.87	43.35	7.10	3.00	0.3885	5.8258	1.1416
MAC-8	23.26	43.20	7.35	2.50	0.3821	6.9873	1.1035

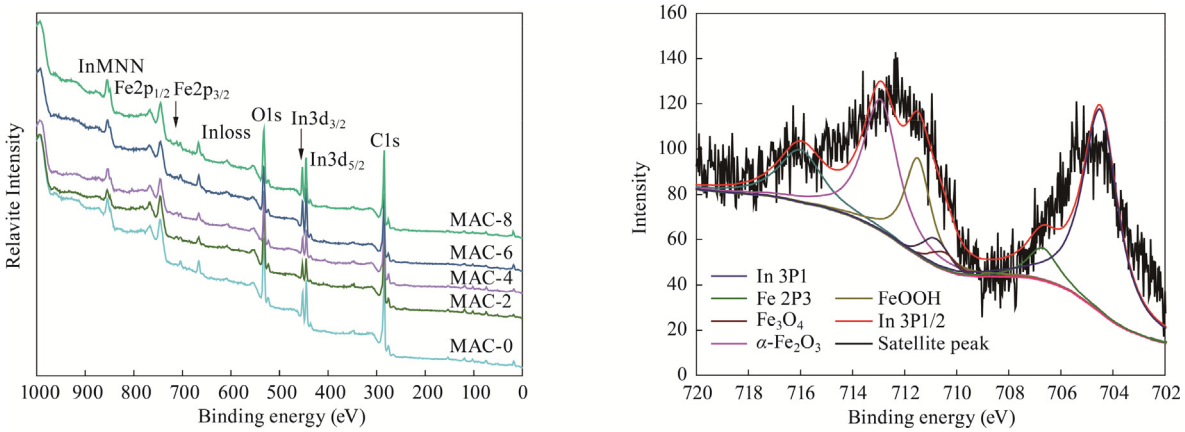

(a) Survey scans of MACs

(b) Fe $2P_{3/2}$ high-resolution spectra of MAC-6

Fig.6. XPS spectra of MACs.

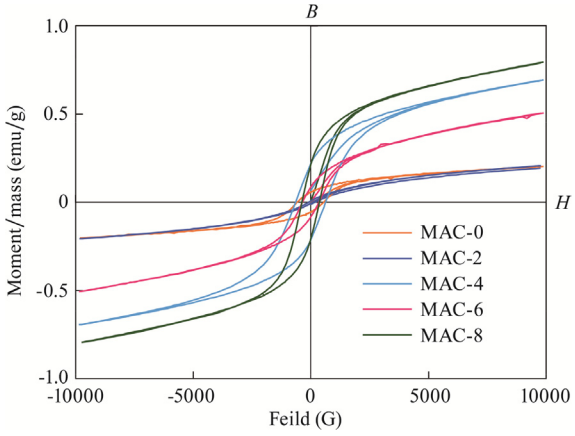

Fig.7. Hysteresis loop of MACs.

of Fe_3O_4 increasing. The value of saturation magnetization M_S of MACs related to the amount of residual Fe_3O_4 and metal Fe in the MACs because they possess a magnetic effect. The specific susceptibility χ of MAC is one of the important parameters for magnetic separation. Once specific susceptibility χ exceeded 1.26×10^{-7}–7.5×10^{-6} $m^3 \cdot kg^{-1}$, MACs can be separated magnetically by a magnetic field of 800–1600 kA/m [16].

There is a significant influence on the coercivity and remanence of prepared magnetic activated carbon in the presence of Fe_3O_4 compared to the reference MAC-0 without Fe_3O_4. The highest coercivity is 644.07 O_e for MAC-4 and the lowest remanence value is 0.084 emu·g^{-1} for the MAC-6. The low value of *Hc* and *Mr* which are close to zero indicate that the MACs exhibited superparamagnetic behaviors at room temperature [18]. The superparamagnetic behavior of the MACs makes it more easily separated by a magnet or a magnetic field. Meanwhile, the low remanence *Mr* largely reduced the aggregation of MACs after it was separated magnetically from the original solution. The result of simple separation tests using a magnet was shown in Fig. 8.

3.5. Transition mechanism of Fe_3O_4 and magnetization of MACs

During the carbonization, the depolymerization process through which gas, water vapor and tar are formed. At the same time, the condensation or repolymerization process occurs [27].

Table 5
Magnetic parameters of MACs.

Sample	Coercivity H_c/O_e	Remanence M_r (emu·g^{-1})	Saturation magnetization M_s (emu·g^{-1})	Specific susceptibility ($\times 10^{-7}\chi$, $m^3 \cdot kg^{-1}$)
MAC-0	571.81	0.06	0.20	9.48
MAC-2	272.52	0.21	0.96	57.2
MAC-4	644.07	0.22	0.69	34.5
MAC-6	351.91	0.084	0.51	20.1
MAC-8	374.88	0.21	0.79	4.11

Note: Specific susceptibilities of all samples were obtained under the magnetic field 120 KA/m (or 1500 Oe).

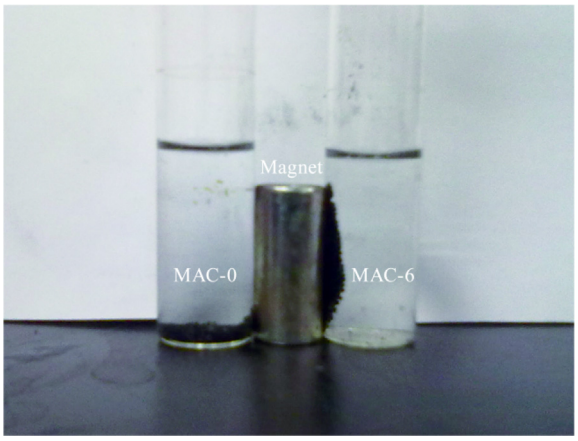

Fig. 8. Magnetic separation tests.

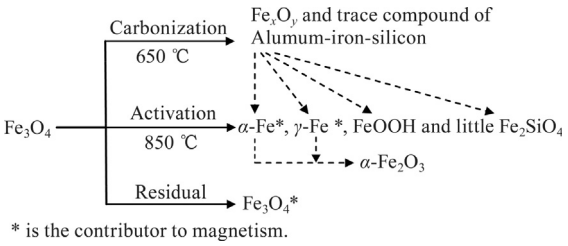

Fig. 9. Transition pattern of Fe_3O_4 during carbonization and activation.

Reduction gas (H_2 and CO) produced from above reactions reacted with Fe_3O_4 and the reactions in Eqs. (1) and (2) happened. Simultaneously, little Al_2O_3 and SiO_2 in the ash reacted with produced FeO to generate a compound of Aluminum-iron-silicon, reaction in Eq. (3) happened [28].

$$Fe_3O_4 + 4H_2 \rightarrow 3FeO + 4H_2O \quad (1)$$

$$Fe_3O_4 + 4CO \rightarrow 3FeO + 4CO_2 \quad (2)$$

$$Al_2O_3 + FeO + SiO_2 \rightarrow \text{Compound of Alumina-iron-silicon} \quad (3)$$

During the activation, steam vapor was used as activation reagent, the overall reaction for non-catalyzed carbon gasification reaction (Eq. (4)) occurred and then in the presence of iron oxides, such a redox cycle has been described in the reactions in Eqs. (5)–(7) [29]. A portion of Fe_xO_y reacted with H_2O to generate FeOOH. From the reaction Eq. (6), it was noticed that the iron oxide could accelerate the burn off of carbon wall.

$$C + H_2O \rightarrow CO + H_2 \quad (4)$$

$$Fe_xO_y + H_2O \rightarrow Fe_xO_y(O) + H_2 \quad (5)$$

$$Fe_xO_y(O) + C_f \rightarrow Fe_xO_y + C(O) \quad (6)$$

$$C(O) \rightarrow C_f + CO \quad (7)$$

When the iron oxides were reduced to iron metal, the following reaction mechanism was proposed as Eqs. (8)–(10) [30,31]. The iron oxides were reduced to α-Fe and γ-Fe. Simultaneously, FeO can react with SiO_2 in the ash to generate Fe_2SiO_4 (see Eq. (11)).

$$Fe + H_2O \rightarrow Fe(O) + H_2 \quad (8)$$

$$Fe(O) + C \rightarrow C(O) + Fe \quad (9)$$

$$C(O) \rightarrow CO \quad (10)$$

$$2FeO + SiO_2 \rightarrow Fe_2SiO_4 \quad (11)$$

The transition mechanism of Fe_3O_4 during the carbonization and activation was shown in Fig. 9. The iron-containing compounds dispersed in the MACs in the major forms of Fe_3O_4, FeO, α-Fe, and γ-Fe, and little Fe_2SiO_4 and trace compound of Aluminum-iron-silicon. This result was in agreement with that of XRD and XPS analysis of MACs. Among these iron-containing compounds, only residual Fe_3O_4 and produced α-Fe and γ-Fe contributed to the magnetism of MACs [8,16,32]. Although partial iron oxide was reduced to metal Fe during the activation, the metal Fe and FeO on the outer surface of MACs were progressively oxidized to α-Fe_2O_3 by air during the storage or use. Compared to the conventional MACs, the MACs prepared by the one-step method have more magnetic stability owing to the magnetic particles was embedded in the MACs.

4. Conclusions

(1) The magnetic granular activated carbon with developed mesoporous structure was successfully prepared by the one-step method. The adsorption capacity and magnetic properties of the MAC with 6 wt% Fe_3O_4 having a specific surface area and mesopore ratio of 370 $m^2 \cdot g^{-1}$ and 55.7% can meet the requirement for the practical application and magnetic recovery.

(2) As a bi-functional additive, Fe_3O_4 could not only accelerate burning off of carbon but also give resultant activated carbon magnetization to render it as a MAC.

(3) During the carbonization and activation, partial Fe_3O_4 changed into FeO, FeOOH, α-Fe, γ-Fe, and a little amount of Fe_2SiO_4 and trace compound of Aluminum-iron-silicon. The residual Fe_3O_4 and metal Fe contribute magnetism to resultant activated carbon.

In the future, the magnetic stability and solubility of compounds containing iron in the MACs as the various acidity of aqueous solution need further investigation.

Acknowledgments

This work was supported by the Fund of 863 High-Tech Research and Development Program of China and the Poten research project No. YA-2016-003.

References

[1] Pietrzak R, Wachowska H, Nowicki P. Preparation of nitrogen-enriched activated carbons from brown coal. Energy Fuels 2006;20(3):1275–80.
[2] Pietrzak R, Wachowska H, Nowicki P, Babel K. Preparation of modified active carbon from brown coal by ammoxidation. Fuel Process Technol 2007;88(4):409–15.
[3] Ariyadejwanich P, Tanthapanichakoon W, Nakagawa K, Mukai SR, Tamon H. Preparation and characterization of mesoporous activated carbon from waste tires. Carbon 2003;41(1):157–64.
[4] Tang L, Zhan L, Yang GZ, Yang JH, Wang YL, Qiao WM, et al. Preparation of mesoporous carbon microsphere/activated carbon composite for electric double-layer capacitors. New Carbon Mater 2011;26(3):237–40.
[5] Hu Z, Srinivasan MP. Mesoporous high-surface-area activated carbon. Micropor Mesopor Mater 2001;43(3):267–75.
[6] Nowicki P, Pietrzak R, Wachowska H. Comparison of physicochemical properties of nitrogen-enriched activated carbons prepared by physical and chemical activation of brown coal. Energy Fuels 2008;22(6):4133–8.
[7] Lin HK, Hill EM, Oleson JL. Recovering gold from carbon fines by a gold transfer process. Miner Metall Process 2003;20(1):47–51.
[8] Oliveira LCA, Rios R, Fabris JD, Garg V, Sapag K, Lago RM. Activated carbon/iron oxide magnetic composites for the adsorption of contaminants in water. Carbon 2002;40(12):2177–83.

[9] Zhu HY, Jiang R, Xiao L, Zeng GM. Preparation, characterization, adsorption kinetics and thermodynamics of novel magnetic chitosan enwrapping nanosized γ-Fe_2O_3 and multi-walled carbon nanotubes with enhanced adsorption properties for methyl orange. Bioresour Technol 2010;101(14):5063–9.
[10] Pardasani D, Kanaujia PK, Purohit AK, Shrivastava AR, Dubey DK. Magnetic multi-walled carbon nanotubes assisted dispersive solid phase extraction of nerve agents and their markers from muddy water. Talanta 2011;86:248–55.
[11] Zhang Z, Kong J. Novel magnetic Fe_3O_4@C nanoparticles as adsorbents for removal of organic dyes from aqueous solution. J Hazard Mater 2011;193:325–9.
[12] Liu ZG, Zhang FS, Sasai R. Arsenate removal from water using Fe_3O_4-loaded activated carbon prepared from waste biomass. Chem Eng J 2010;160(1):57–62.
[13] Yang N, Zhu SM, Zhang D, Xu S. Synthesis and properties of magnetic Fe_3O_4-activated carbon nanocomposite particles for dye removal. Mater Lett 2008;62(4–5):645–7.
[14] Zhang J, Xie Q, Liu J, Yang MS, Yao X. Role of $Ni(NO_3)_2$ in the preparation of a magnetic coal-based activated carbon. Min Sci Technol 2011;21(4):599–603.
[15] Ao YH, Xu JJ, Fu DG, Yuan CW. A simple route for the preparation of anatase titania-coated magnetic porous carbons with enhanced photocatalytic activity. Carbon 2008;46(4):596–603.
[16] Yang MS, Xie Q, Zhang J, Liu J, Wang Y, Zhang XL, et al. Effects of coal rank, Fe_3O_4 amounts and activation temperature on the preparation and characteristics of magnetic activated carbon. Min Sci Technol 2010;20(6):872–6.
[17] Ai LH, Huang HY, Chen ZL, Wei X, Jiang J. Activated carbon/$CoFe_2O_4$ composites: facile synthesis, magnetic performance and their potential application for the removal of malachite green from water. Chem Eng J 2010;156(2):243–9.
[18] Ao YH, Xu JJ, Shen XW, Fu DG, Yuan CW. Magnetically separable composite photocatalyst with enhanced photocatalytic activity. J Hazard Mater 2008;160(2–3):295–300.
[19] Wang SH, Zhou SQ. Titania deposited on soft magnetic activated carbon as a magnetically separable photocatalyst with enhanced activity. Appl Surf Sci 2010;256(21):6191–8.
[20] Yamashita T, Hayes P. Analysis of XPS spectra of Fe^{2+} and Fe^{3+} ions in oxide materials. Appl Surf Sci 2008;254(8):2441–9.
[21] Hu Z, Srinivasan MP, Ni Y. Novel activation process for preparing highly microporous and mesoporous activated carbons. Carbon 2001;39(6):877–86.
[22] Nowicki P, Pietrzak R, Wachowska H. X-ray photoelectron spectroscopy study of nitrogen-enriched active carbons obtained by ammoxidation and chemical activation of brown and bituminous coals. Energy Fuels 2010;24(2):1197–206.
[23] Yu JL, Tian FJ, Chow MC, McKenzie LJ, Li CZ. Effect of iron on the gasification of Victorian brown coal with steam: enhancement of hydrogen production. Fuel 2006;85(2):127–33.
[24] Maahs HG. Crystallite parameter correlations for graphitic carbons. Carbon 1969;7(4):509–10.
[25] Gong GZ, Xie Q, Zheng YF, Ye SF, Chen YF. Regulation of pore size distribution in coal-based activated carbon. New Carbon Mater 2009;24(2):141–6.
[26] Grosvenor AP, Kobe BA, Biesinger MC, Mclntyre NS. Investigation of multiplet splitting of Fe 2p XPS spectra and bonding in iron compounds. Surf Interface Anal 2004;36(12):1564–74.
[27] Seo DK, Park SS, Kim YT, Hwang JH, Yu TU. Study of coal pyrolysis by thermogravimetric analysis (TGA) and concentration measurements of the evolved species. J Anal Appl Pyrol 2011;92(1):209–16.
[28] Huffman GP, Huggins FE, Dunmyre GR. Investigation of the high-temperature behaviour of coal ash in reducing and oxidizing atmospheres. Fuel 1981;60(7):585–97.
[29] Yamashita H, Ohtsuka Y, Yoshida S, Tomita A. Local structures of metals dispersed on coal. 1. Change of local structure of iron species on brown coal during heat treatment. Energy Fuels 1989;3(6):686–92.
[30] Hermann G, Huttinger KJ. Mechanism of iron-catalyzed water vapour gasification of carbon. Carbon 1986;24(4):429–35.
[31] Li J, Li BW, Zhang BW. Microwave carbothermic reduction from Fe_2O_3 to Fe_3O_4 powders. J Univ Sci Technol Beijing 2011;33(9):1127–32.
[32] Marcilla A, Asensio M, Gullon MI. Influence of the carbonization heating rate on the physical properties of activated carbons from a sub-bituminous coal. Carbon 1996;34(4):449–56.